crystals

MDPI

Article

Layer-by-Layer Extracellular Biological Synthesis of Sustainable Ag-Based Nanoparticles for Catalytic Reduction of Methylene Blue Dye

Mohamed G. M. Kordy [1,2,*], Inas A. Ahmed [3], Mohammed Abdel-Gabbar [1], Hanan A. Soliman [1], Abeer S. Altowyan [4] and Mohamed Shaban [2,5,*]

[1] Biochemistry Department, Faculty of Science, Beni-Suef University, Beni-Suef 62521, Egypt
[2] Nanophotonics and Applications (NPA) Lab, Physics Department, Faculty of Science, Beni-Suef University, Beni-Suef 62514, Egypt
[3] Department of Chemistry, Faculty of Science, King Khalid University, Abha 62224, Saudi Arabia
[4] Department of Physics, College of Science, Princess Nourah bint Abdulrahman University, Riyadh 11671, Saudi Arabia
[5] Department of Physics, Faculty of Science, Islamic University of Madinah, Madinah 42351, Saudi Arabia
* Correspondence: m.kordybio@science.bsu.edu.eg (M.G.M.K); mssfadel@aucegypt.edu (M.S.)

Abstract: Novel cubic microstructures for the purposes of plasmonic Ag-based NPs were made using biological wastes produced from a microbial culture of *Bacillus cereus* (*B. cereus*) employing a bottom-up approach for the biosynthesis of metal-based nanomaterials. The unique surface plasmon resonance (SPR) of the as-prepared Ag-based NPs was detected at 405 nm. The infra-red spectrum revealed that the used biological waste effectively stabilized our Ag-based NPs. Scanning and transmission electron microscopes were used in order to evaluate the sizes and shapes of the distinctive structures present in our samples. The Ag NPs had a face-centered cubic structure, with a size of 64.4 nm for the (200) nano-crystallites, according to the X-ray diffraction that was conducted. The zeta potential was found to be −19.5 mV and the dynamic light scattering (DLS) size was 238.8 nm. Methylene blue's (MB) reaction with $NaBH_4$ was used in order to measure the catalytic activity of the generated Ag-based NPs over a period of 1 to 5 min. With an astonishing reaction rate of 0.2861 min^{-1}, the MB elimination percentage reached 67% in just 5 min, displaying outstanding catalytic activity. This work can therefore encourage the use of this biowaste for the ecologically benign, cost-effective, and long-term synthesis of innovative Ag-based nanoparticles and nanostructures, as well as in their use as catalysts in the catalytic reduction in MB.

Keywords: $AgNO_3$; Ag; biosynthesis; *Bacillus cereus*; Ag-based nanoparticles; face-centered cubic; sustainable development goals; biological waste; cubic microstructures

Citation: Kordy, M.G.M.; Ahmed, I.A.; Abdel-Gabbar, M.; Soliman, H.A.; Altowyan, A.S.; Shaban, M. Layer-by-Layer Extracellular Biological Synthesis of Sustainable Ag-Based Nanoparticles for Catalytic Reduction of Methylene Blue Dye. *Crystals* **2022**, *12*, 1576. https://doi.org/10.3390/cryst12111576

Academic Editor: Ferdinando Costantino

Received: 23 September 2022
Accepted: 28 October 2022
Published: 4 November 2022

1. Introduction

The molecular structure of materials is often altered through nanotechnology in order to produce intelligent materials that can be employed in a variety of applications [1,2]. Due to their distinctive physical and biochemical properties at the nano size, these nanostructured materials have become a reliable platform for numerous applications, including energy, food, and environmental science [3–5]. Nanomaterials are substances that are generated as single units and have at least one dimension between 1 and 100 nm [6]. Inorganic nanoparticles, carbon-based nanomaterials, organic-based nanomaterials, and composite-based nanomaterials are the four types of nanomaterials that can be distinguished [7–10]. The more attractive type is made up of inorganic-based nanomaterials such as silver (Ag), which is the subject of our study. Silver has potent catalytic, antibacterial, and antioxidant properties; further, it can be used to treat and diagnose cancer [5,11–13]. Ag NPs may be synthesized by biological, chemical, or physical methods [14]. In contrast to chemical and

physical methods, the biosynthesis of nanostructures by microorganisms or plant extracts results in more predictable sizes and also forms in regard to the nanoparticles. Further, it does not require the use of hazardous and dangerous substances [15]. In the biosynthesis of Ag NPs specifically, reducing and capping agents are mostly derived from microorganisms and plant extracts. Without the use of additional capping agents, microorganism-based biosynthesis generates internal and extracellular assemblies within stable Ag NPs [16].

Microorganisms can recycle environmental nutrients by decomposing organic matter. Domestic and industrial waste removal is also carried out by microbes that decompose organic materials, such as animal carcasses and tree trunks [17]. Additionally, inefficient—and inadequate—solid and liquid waste management has an impact on the environment, not only locally but also regionally and worldwide [18]. Therefore, using waste from biological culturing in order to make nanomaterials is another way to dispose of undesirable compounds that are obtained from bacteria via biological synthesis. Due to this, synthesizing nanomaterials from biological waste helps achieve sustainable development goals (SDGs), as opposed to the alternative physical and chemical approaches, which only rely on expensive and finite resources.

On the other hand, it is essential to clean dye effluents before releasing them into receiving water as many dyes have poor biodegradability and are extremely carcinogenic. Chemical procedures, such as chlorination and ozonation, as well as physical tactics, such as adsorption, are among the most sophisticated technical options for the conveyance of these contaminants [19]. In this work, we intend to advance innovative Ag-based nanoparticles and nanostructures for use as efficient and sustainable catalysts that are environmentally benign, commercially feasible, and long-lasting for the catalytic reduction in MB dye. Here, a bottom-up strategy for the biosynthesis of metal-based nanomaterials was used in order to produce novel cubic microstructures of the plasmonic Ag-based NPs, while using biological wastes generated from a microbial culture of *Bacillus cereus* (*B. cereus*). With the help of UV/Vis, FTIR, SEM, TEM, XRD, DLS size, zeta potential, and EDAX techniques, the Ag-based NPs were characterized. Moreover, the biosynthesized Ag-based NPs' catalytic activity was evaluated against MB dye.

2. Materials and Methods

2.1. Materials

A 2 mM solution prepared from silver nitrate ($AgNO_3$) (purity of 99.9%) was purchased from TITAN, India. The *B. cereus* strain was obtained from RCMB, Al-Azhar University in Cairo, Egypt. Nutrient Broth was bought from Himedia, India. Al-Nasr Company's methylene blue (MB) dye was utilized (Giza, Egypt). Sodium borohydride ($NaBH_4$) was purchased from Research Lab Fine Chem Industries (Mumbai, India). All studies were conducted using double-distilled water.

2.2. Method

2.2.1. Preparation of the Bio-Waste from the Culturing Medium of *B. Cereus*

The pure culture inoculum of *B. cereus* was introduced into a 250 mL and 100 mL sterilized, 25 g/L nutritious broth contained in an Erlenmeyer flask. The liquid culture was kept at 28 °C for 48 h using a shaking incubator with 180 rpm. The produced culture was centrifuged using a cooling centrifuge at 4000 rpm at 4 °C. The obtained supernatant (bio-waste), i.e., the source of reducing and stabilizing agents, was subjected to the biosynthesis of our nanostructures, as shown in Figure 1.

2.2.2. Synthesis of Bio-Waste Ag-Based NPs

A total of 34 mg of $AgNO_3$ is dissolved in 100 mL of deionized water using magnetic stirring at 300 rpm for 10 min in order to produce a 2 mM $AgNO_3$ solution. Then, equal volumes of the two reactants of bio-waste and 2 mM $AgNO_3$ solution (100 mL of each reactant) are mixed in a suitable container. The mixture's pale yellow color changed to a dark reddish brown in 10 min while being kept at an ambient temperature and in

complete darkness. This change was evidence of the synthesis of our bio-waste Ag-based NPs. The color shift was confirmed by examining the absorption peak using a UV/Vis spectrophotometer (Lambda 950, Perkin Elmer, Boston, MA, USA).

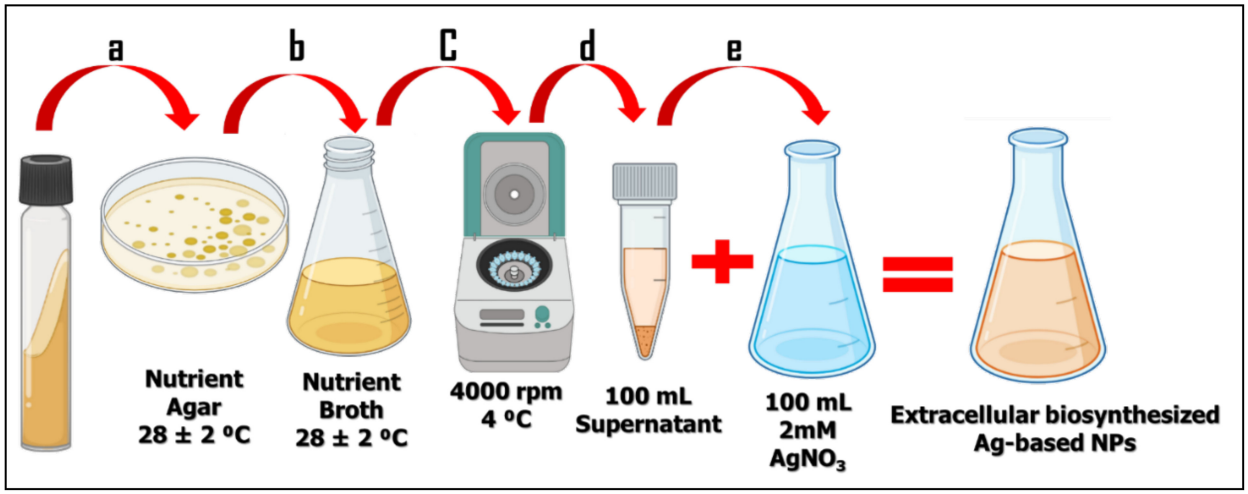

Figure 1. The entire process of the extracellular biosynthesis of Ag-based NPs utilizing sustainable bio-waste including all steps (**a**–**e**).

2.2.3. Characterization of the Bio-Waste Ag-Based NPs

The FTIR (8400 S Shimadzu, Kyoto, Japan) spectrophotometer made it possible to detect the functional groups that increased the stability of bio-waste Ag-based NPs. The size and morphological studies were revealed using SEM (JSM 6510, JEOL, Tokyo, Japan) and TEM (JEOL 2010F, JEOL, Tokyo, Japan). Image-J software was used to determine the particle diameter distributions and size histograms from TEM and SEM images [20]. The elemental analysis of bio-waste Ag-based NPs was determined using SEM–EDAX instrumentation (JED 2300, JEOL, Tokyo, Japan). The distribution of particle diameters was also confirmed using dynamic light scattering (DLS). The zeta potential further dictated the stability using a Zetasizer (Nano ZS90, Malvern, UK). Notably, the sample was placed on a glass slide for investigations using the SEM, EDAX, and XRD.

2.2.4. Catalytic Dye Degradation of MB Activity

The catalytic reduction of 1 mL of 5 ppm MB by 100 µL of the as-prepared Ag-based NP liquid was tested utilizing 1 mL of 0.1 M $NaBH_4$ (Research Lab Fine Chem Industries, Mumbai, India). In order to capture the whole UV/Vis spectrum from 550 to 750 nm, the test samples were made by adding these specific volumes to cuvette samples, followed by time monitoring every minute.

Equations (1) and (2) were used in order to compute the catalytic reduction percentage and reduction rate of MB. To apply pseudo-first-order kinetics and to obtain the reduction rate, Equation (2)'s linear relationship between $\ln\left(\frac{A_o}{A_t}\right)$ and reduction time (min) is used.

$$\text{Catalytic reduction } \% = \frac{A_o - A_t}{A_t} \times 100 \quad (1)$$

$$\ln\left(\frac{A_o}{A_t}\right) = k_{app}t \quad (2)$$

where A_o and A_t refer to the absorbance of MB at the start and (1, 2, 3, 4, and 5) min, respectively, at a single wavelength (660 nm).

3. Results and Discussions

3.1. Characterization of the Bio-Waste Ag-Based NPs

The UV/Vis spectrum demonstrated that the Ag-based NPs were successfully synthesized from bio-waste. The mixture's color changed from pale yellow to dark brown, which is the first sign that Ag NPs are being biosynthesized. Two peaks in the UV/Vis spectrum were seen at λ~263 and 405 nm. The SPR that corroborated the presence of the biosynthesized Ag-based NPs utilizing the bio-waste was detected at 405 nm, as shown in Figure 2A. As the conduction and valence bands are close together and allow the electrons to move about easily, metal nanoparticles exhibit exceptional light absorption. When the electromagnetic field's frequency and the surface plasmon resonance (SPR) frequency of the free electron in the NPs coincide, there is a significant absorption. The dielectric medium, particle size, and chemical components all significantly affect this absorption [21]. The UV/Vis spectrum study may also indicate that the Ag-based NPs produced by biosynthesis are anisotropic and small [15]. Further, the broad SPR band is due to the anisotropic nature of the particles. These results were quite similar to that noted by Alfryyan et al. [22], Taboada-López et al. [23], Alsamhary et al. [11], and Picoli et al. [24]. This result was also relevant to those obtained by Paulkumar et al. [25], who synthesized the AgCl NPs using *B. subtilis* in 2013. According to Paulkumar et al., silver chloride nanoparticles were produced as a result of the presence of chloride ions from sodium chloride in the nutrient broth used for bacterial growth, which is why the prepared particles absorb light at 405 nm in our study. We believe that these Ag-based NPs are fairly equivalent to Ag/AgCl NPs.

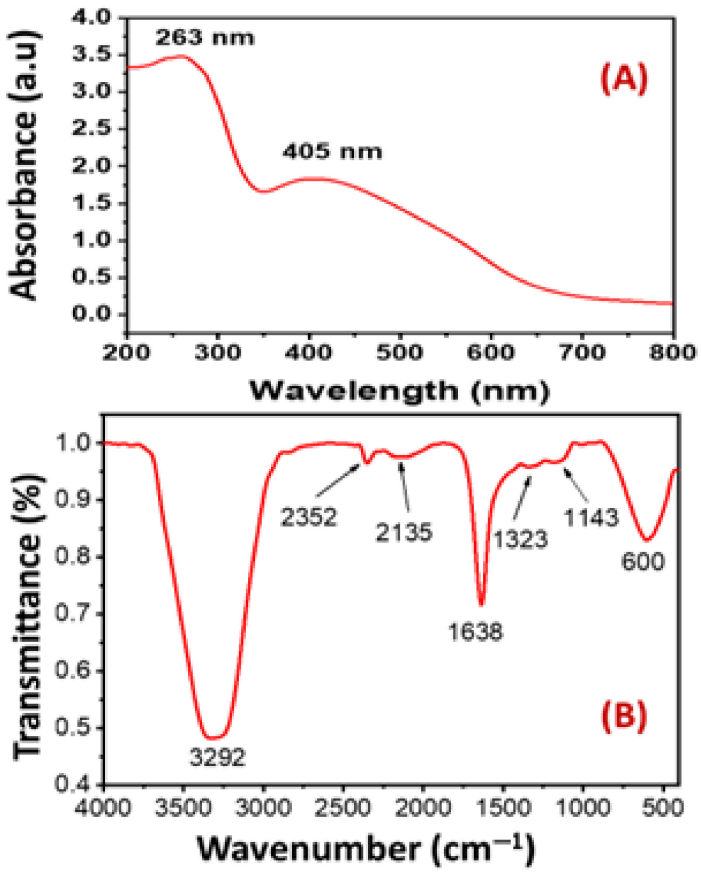

Figure 2. (**A**) is the UV/Vis spectrum and (**B**) is the FTIR spectrum of bio-waste Ag-based NPs.

The IR spectrum demonstrated the existence of the stabilizing agents in the produced Ag-based NPs. The bacterial medium bio-waste was obtained after removing the culture of *B. cereus* using this medium as a method of sustainable fabrication. Utilizing hazardous

waste that is considered a non useful component can be used to produce various types of NPs. Indeed, it is this process that is chosen in this paper.

In Figure 2B, the IR spectral analysis was conducted in order to determine the potential functional groups that are in charge of reducing Ag^+ ions to Ag, as well as the formation of silver chloride nanoparticles in order to identify the capping and efficient stabilization agents in the biosynthesized Ag NP samples. The IR spectrum showed the observed peaks' intensities at 3292, 2352, 2135, 1638, 1323, 1143, and 600 cm^{-1}.

Among these peaks, there are four distinctive peaks, that is: (I) The bands at 3292 cm^{-1} are attributed to the O–H stretch that is intermolecular bonded as well as some free amide I (N–H) bending. (II) The band at 2352 cm^{-1} is attributed to a C–O vibrational stretch that verifies the existence of additional carbonyl groups (C=O), such as carboxylic, ketonic, and aldehydic groups in the sample of carboxylic and amino acids, amides, or saccharides—which are in charge of reducing Ag^+ ions. (III) The band at 1638 cm^{-1} could be allocated to the N–H stretching vibrations of primary amines. (IV) The band at 600 cm^{-1} may be attributed to halides, such as chloride, that are present in the tested sample. In comparing these results with the recently published paper in 2022 [22], the IR study of extracellular Ag NPs is quite similar to our biosynthesized sample. This may be due to using the same mechanism of synthesis, however they are different in the used concentration of Ag^+ ions. Here, we can notice that the peak at 2352 cm^{-1} is minimized with the higher concentration of Ag^+, which may lead to confirming the assumption of participation of the C–O groups in reducing Ag^+ and stabilizing the Ag NPs.

SEM micrographs revealed the presence of the microstructures with different dimensions in Figure 3A. The notable shapes in Figure 3B were clearly cubes with a centered, internal, tetrahedron, and pyramidal hollow shape (i.e., a tunnel-like structure). In Figure 3C, the rough surface of these cuboidal structures reveals a good indication of the spherical shape of our Ag NPs. This may lead to a rise in the surface area of our produced Ag-based NPs and hence the increase in the catalytic activity. These Ag NPs were well aligned and organized on the surface of the notable cubes. These notable cubes were similar to that which were observed by Wu et al. in 2015 [26]. Large numbers of Ag nanocubes with good homogeneity were produced by enhancing the oxidative etching impact of Br ions during the polyol synthesis.

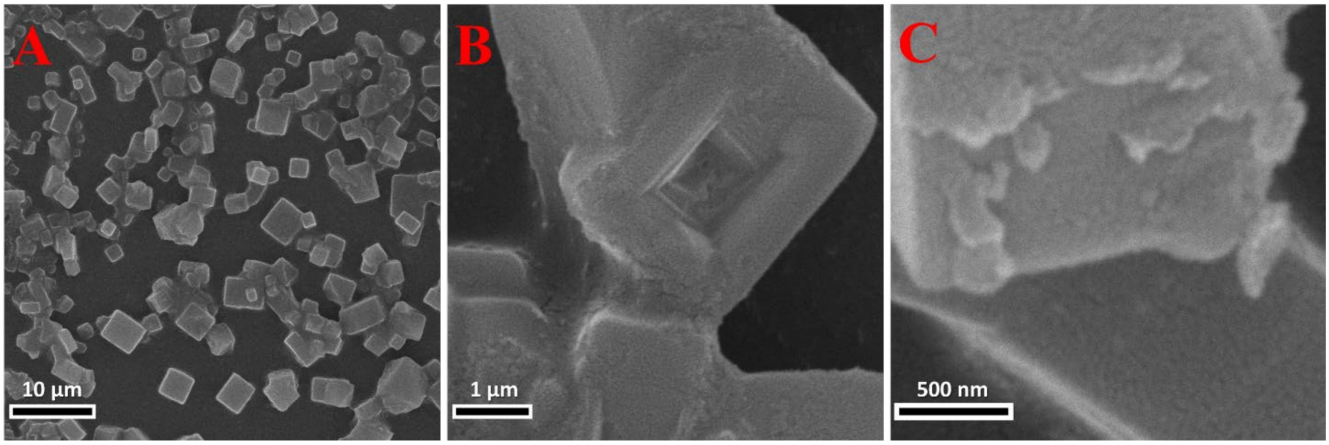

Figure 3. (**A**–**C**) are SEM images of the prepared sample with different scale bars and magnifications.

Therefore, we can assume that Cl^- caused the same effect as Br^- ions in the bioreduction process for the notable cubes. The heating of the slide onto the hot plate for 10 min removed the organic template, this is for the formation of the hollow shapes in the notable cubes. The overall process can be defined as selective self-assembly of Ag NPs in which layer-by-layer self-assembly results in rectangular and squared micro pits of average dimensions of 1.8 µm, as shown in Figure 4 in regard to the sharp edges.

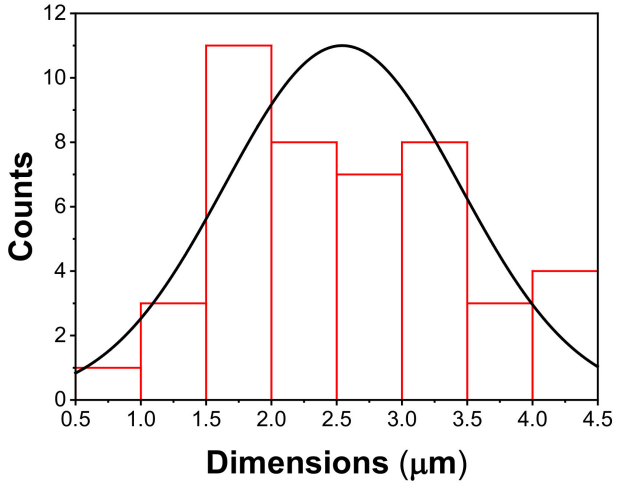

Figure 4. Histogram of dimensions of the notable cubes in μm from Figure 3A.

The square shape of the biosynthesized microstructures was evident in the TEM image of Figure 5A. The particle size distribution, shown in Figure 5B, shows that the size is distributed throughout a range of 182.6 to 381.9 nm, with an average value of 267.6 nm. These particles were observed with no aggregations and were relatively greater than those reported by Sharifi-Rad and Pohl [27]. In addition, we noticed that these structures were condensed from the edges and therefore possessed a less condensed intensity in the center, which confirms the presence of hollow shapes in these notable cubes in the SEM images.

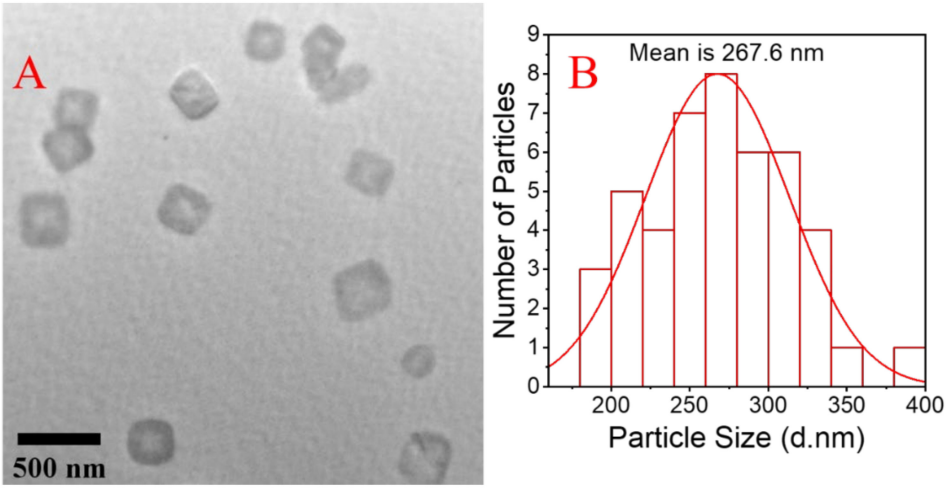

Figure 5. (**A**) TEM image of the prepared sample and (**B**) histogram of the notable microstructures' dimensions.

Figure 6 shows an evaluation of the crystallographic features of biosynthesized Ag-based NPs that are utilizing XRD. The main characteristic peaks were at 2θ values of 31.53°, 45.31°, 56.28°, and 66.05°. They corresponded to (200), (220), (311), and (400) planes, correspondingly. These peaks belong to the face-centered cubic (FCC) structure of AgCl, according to the JCPDS card No.31-1238 [28], i.e., the XRD data confirm the production of biogenic Ag-based NPs with a face-centered cube structure using B. cereus culture waste and 2 mM $AgNO_3$.

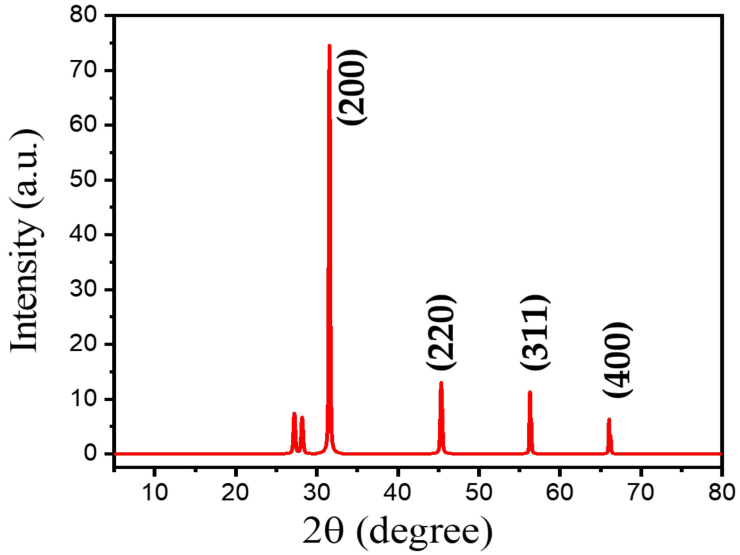

Figure 6. XRD pattern of biosynthesized Ag-based NPs using the waste of *B. cereus* culturing.

Using the Scherrer equation, the crystallite size (CS) was determined from the XRD chart [29,30]. Williamson and Smallman's relation, $\delta = \frac{1}{CS^2}$, is used in order to compute the minimum dislocation density (δ). Table 1 includes the computed values for the crystallite size (CS), d-spacing, dislocation density, and microstrain. This is in addition to the estimated values for FWHM and the relative intensity of the four highest peaks in the XRD chart. The (200) orientation has the largest reported value (2.837 Å) of d-spacing, while the (400) plane has the lowest reported value (1.415 Å). The value of the crystallite along the optimum orientation was discovered to be 64.6 nm (200). Dislocation density values ranged from 0.831×10^{-4} nm^{-2} for (400) to 3.684×10^{-4} nm^{-2} for (220). A high degree of crystallinity along the (200) plane is present in the produced nano-crystallites, according to the XRD investigation [31]. With regard to non-uniform lattice distortions, faulting, dislocations, antiphase domain boundaries, and grain surface relaxation, the greatest microstrain % recorded was at 0.21954% for the preferred orientation (200) [32].

Table 1. Values of FWHM, relative intensity, the crystallite size (CS), d-spacing, dislocation density, and microstrain.

Pos. [°2Th.]	FWHM [°2Th.]	Rel. Int. [%]	[hkl]	d-Spacing [Å]	Cs [nm]	Dislocation Density [nm^{-2}]	Microstrain [%]
31.53	0.1574	100	(200)	2.837	64.6	2.396×10^{-4}	0.21954
45.31	0.1968	18.08	(220)	2.001	52.1	3.684×10^{-4}	0.19203
56.28	0.1181	20.08	(311)	1.634	102.9	0.944×10^{-4}	0.07944
66.05	0.1181	10.7	(400)	1.415	109.7	0.831×10^{-4}	0.06448

The Ag and AgCl nanostructures, which were synthesized using *B. cereus* were also identified by EDX analysis, which supported the silver ion reduction. The emission peaks were recorded almost at 3 keV (Lα, $L\beta_1$, and $L\beta_2$), which is obvious for the purposes of silver nanocrystal creation in Figure 7. The EDX spectrum has shown silver peaks along with sodium, silicon, carbon, potassium, oxygen, and chlorine peaks. The chlorine and oxygen peaks may be attributed to biomolecules that were present with carbonaceous compounds on the surface of Ag and AgCl nanostructures or due to the chlorine on the glass slides that were used for sample preparation along with sodium and silicon high %.

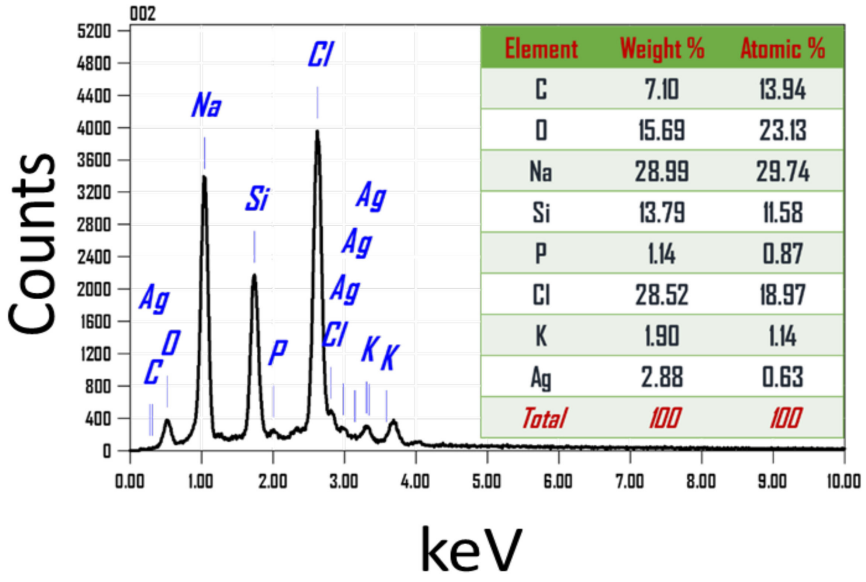

Figure 7. EDX chart of biosynthesized Ag-based NPs using bio-waste of *B. cereus* culturing.

The DLS size was measured in Figure 8 with an average size of 238.8 nm, a polydispersity index (PDI) of 0.47, and a zeta potential of −19.5 mV. These results indicate that the size was more relevant to those identified by TEM images. Further, the nanoparticles with PDI less than 0.5 are monodisperse and may be less aggregated. The zeta potential also indicated the good stability of our produced Ag-based NPs that were synthesized by the bio-waste of *B. cereus* culture. This is good and enhances the idea of the capability of the used bio-waste for the reduction in Ag^+ ions as well as the stabilization of the produced Ag NPs.

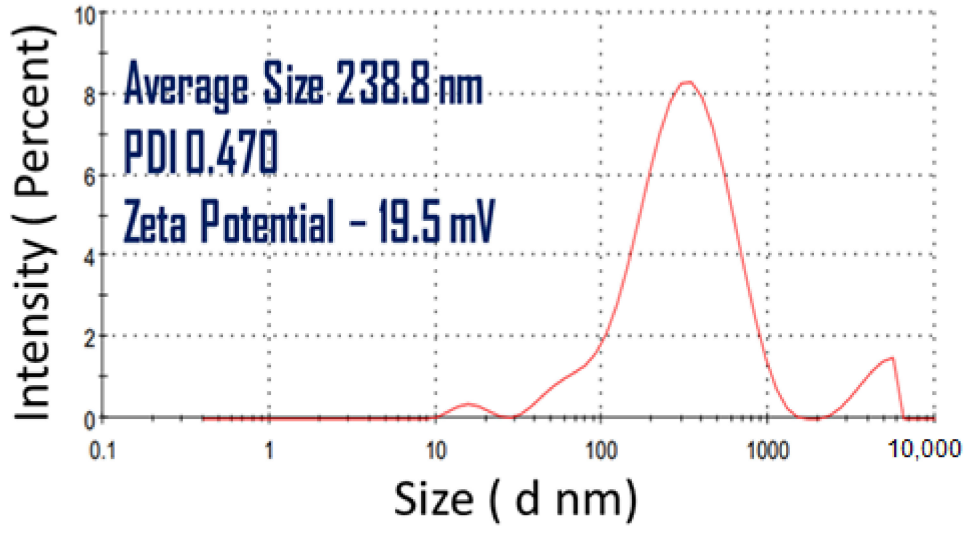

Figure 8. DLS size of Ag-based NPs that are prepared by using bio-waste.

3.2. Catalytic MB Dye Degradation Activity

The MB dye is blue in color, and it reduces via $NaBH_4$ into leuco-MB, which is colorless. This reaction can be accelerated by using our Ag-based NPs, which are biosynthesized via a biological waste culture of *B. cereus*, which also makes them sustainable NPs. Ag NPs are well known for their ability to assist in the transfer of electrons from BH_4^- (the electron donor) to MB (the electron acceptor). In comparison to Ag NPs, MB (a cationic dye) is electrophilic, while BH_4^- ions are nucleophilic. As a result, as shown in the scheme in

Figure 9, the Ag NPs receive electrons from BH_4^- ions and transmit them to the MB. From time 1 to 5 min—i.e., the stability condition—the catalytic activity of our Ag-based NPs was studied for the MB reaction with $NaBH_4$ at an absorbance of 660 nm in Figure 10A. After applying Equations (1) and (2), Figure 10B,C, they demonstrated a very efficient catalyst with a 67% degradation of MB dye and a rate constant of 0.2861 min^{-1} with R^2 0.97034. These results show a high catalytic reduction in MB as compared with other Ag-based NPs as mentioned in research [22] depending on the value of the reaction rate constant.

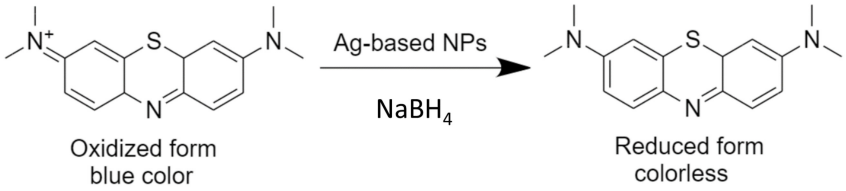

Figure 9. Schematic of reduction reaction of MB dye using $NaBH_4$ in the presence of our sustainable Ag-based NPs catalyst.

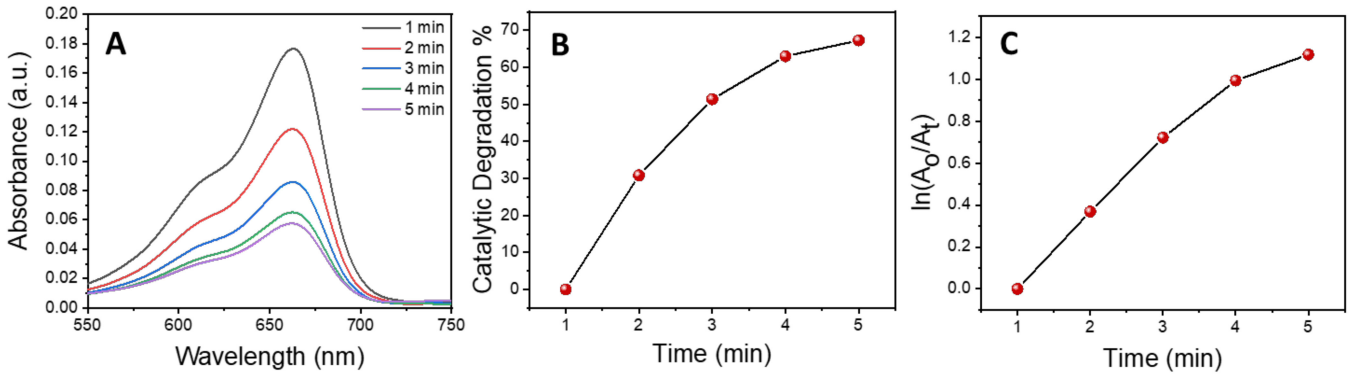

Figure 10. (**A**) Absorption spectra of MB solution at various reaction times in the existence of Ag-based NPs, (**B**) the catalytic reduction (expressed in %) versus time, and (**C**) the first-order kinetic modeling.

It is clear from Figure 10C that the reduction in MB occurs catalytically and follows a pseudo-first-order reaction kinetic due to the linear relationship between $\ln\left(\frac{A_0}{A_t}\right)$ and t (min). The rate constant was obtained from the slope of the linear segment of this graph and presented, as expressed in Equation (3).

$$y = 0.2861\ x - 0.21783 \quad (3)$$

Compared to green coffee-capped Ag NPs [5], the rate of MB reduction from our sustainable Ag-based NPs was significantly higher due to the Ag NPs' rough surface, high surface area, and increased negative potential, which are organized into layers and hollow forms, as shown in Figure 3B,C. Moreover, E° (MB) = + 0.01 V > E° (Ag-based NPs) = − 0.0195 V > E° (BH_4^-) = − 0.21 V, which exemplifies the perfect circumstances for a successful relay of electrons between the acceptor (MB) and the donor ($NaBH_4$). As a result—compared to other electrophiles, including those reported in studies by Kordy et al. [5]—our sustained Ag-based NPs were able to take electrons from BH_4^- and transfer them to MB more quickly. Regarding reaction and performance parameters, Table 2 compares our bio-waste Ag-based NPs with previously reported Ag-based nano-catalysts [5,22,33]. In contrast to previously reported values for *B. cereus* intracellular Ag NPs or *B. cereus* extracellular Ag NPs, this table clearly demonstrated that our bio-waste Ag-based NPs have a high-rate constant toward the removal of MB [22].

Table 2. Comparison between different fabricated Ag-based nano-catalysts and our bio-waste Ag-based NPs concerning reaction and performance parameters.

The Used Ag-Based NPs Catalyst	Catalyst Volume or Quantity	Dye, Concentration, and Volume	Reductant, Concentration, and Volume	k_{app} (min^{-1})	Time (min)	Ref.
B. cereus intracellular Ag NPs	100 µL	MB, 50 ppm, and 25 mL	$NaBH_4$, 0.1 M, and 5 mL	0.00641	150	[22]
B. cereus extracellular Ag NPs	100 µL	MB, 50 ppm, and 25 mL	$NaBH_4$, 0.1 M, and 5 mL	0.04972	80	
GC-capped Ag NPs	100 µL	MB, 50 ppm, and 1 mL	$NaBH_4$, 0.1 M, and 1 mL	0.2867	12	[5]
Fe_3O_4@SiO_2/Ag nanocomposite	0.002 g	MB, 0.00005 M	Photocatalytic	1.58 ± 0.09	14	[33]
Bio-waste of *B. cereus* culture Ag-based NPs	100 µL	MB, 5 ppm, and 1 mL	$NaBH_4$, 0.1 M, and 1 mL	0.2861	4	This work

4. Conclusions

An innovative bottom-up method for the biosynthesis of metal-based nanomaterials has been applied in order to produce novel cubic microstructures for plasmonic Ag-based NPs, while utilizing biological waste from a *Bacillus cereus* microbial culture. The characteristic SPR of plasmonic Ag-based NPs was detected at 405 nm beside a new apparent peak at 263 nm. The infra-red spectrum demonstrated that the biological waste was successfully used in order to stabilize the generated Ag-based NPs. According to TEM analysis, the remarkable microcubes had an average size of 267.6 nm. XRD was used in order to identify the FCC structure of Ag NPs, which possessed nanocrystallites with an average size of 64.4 nm. The zeta potential was found to be −19.5 mV. The DLS size was determined to be 238.8 nm, which is consistent with the results of the TEM analysis. The catalytic activity of the produced Ag-based NPs was evaluated over a time range of 1 to 5 min, using the reaction of MB with $NaBH_4$. The MB elimination percentage reached 67% after 5 min with an astounding reaction rate of 0.2861 min^{-1}, demonstrating exceptional catalytic activity. This study can therefore promote the use of bio-waste for the environmentally friendly, economically viable, and long-term synthesis of novel Ag-based nanoparticles and nanostructures, as well as their application as catalysts in the catalytic reduction in dyes.

Author Contributions: Conceptualization, M.G.M.K., M.A.-G., H.A.S., I.A.A., A.S.A. and M.S.; methodology, M.G.M.K. and M.S; software, M.G.M.K.; validation, M.A.-G., H.A.S., A.S.A. and M.S.; formal analysis, M.G.M.K., I.A.A., A.S.A. and M.S.; investigation, M.G.M.K., A.S.A. and M.S.; resources, M.G.M.K., I.A.A., A.S.A. and M.S.; data curation, M.G.M.K., M.A.-G., H.A.S., A.S.A. and M.S.; writing—original draft preparation, M.G.M.K. and M.S.; writing—review and editing, M.G.M.K., M.A.-G., H.A.S., I.A.A., A.S.A. and M.S.; visualization, M.A.-G., H.A.S., I.A.A., A.S.A. and M.S.; project administration, M.G.M.K., I.A.A., A.S.A. and M.S.; funding acquisition, M.G.M.K., M.S., A.S.A. and I.A.A. All authors have read and agreed to the published version of the manuscript.

Funding: Funding was received from the Dean of Science and Research at King Khalid University via the General Research Project: Grant no. (R.G.P.1/320/43). This research was also funded by Princess Nourah bint Abdulrahman University Researchers Supporting Project number (PNURSP2022R16), Princess Nourah bint Abdulrahman University, Riyadh, Saudi Arabia. Additionally, this research received external funding from the Egyptian Academy of Scientific Research and Technology, which partially supported this work (SNG-2015-108).

Institutional Review Board Statement: Not applicable.

Informed Consent Statement: Not applicable.

Data Availability Statement: The data presented in this study are available on request from the corresponding authors.

Acknowledgments: The authors express their gratitude to the Dean of Science and Research at King Khalid University for giving financial support(R.G.P.1/320/43). The authors like to express their gratitude to Princess Nourah bint Abdulrahman University Researchers Supporting Project number (PNURSP2022R16), Princess Nourah bint Abdulrahman University, Riyadh, Saudi Arabia. Additionally, the authors gratefully acknowledge the financial support from the Egyptian Academy of Scientific research and Technology, which partially supported this work (SNG-2015-108).

Conflicts of Interest: The authors declare no conflict of interest.

References

1. Shaban, M.; Almohammedi, A.; Saad, R.; El Sayed, A.M. Design of SnO_2:Ni,Ir Nanoparticulate Photoelectrodes for Efficient Photoelectrochemical Water Splitting. *Nanomaterials* **2022**, *12*, 453. [CrossRef] [PubMed]
2. Saad, R.; Gamal, A.; Zayed, M.; Ahmed, A.M.; Shaban, M.; BinSabt, M.; Rabia, M.; Hamdy, H. Fabrication of ZnO/CNTs for Application in CO_2 Sensor at Room Temperature. *Nanomaterials* **2021**, *11*, 3087. [CrossRef] [PubMed]
3. Rabie, A.M.; Shaban, M.; Abukhadra, M.R.; Hosny, R.; Ahmed, S.A.; Negm, N.A. Diatomite supported by CaO/MgO nanocomposite as heterogeneous catalyst for biodiesel production from waste cooking oil. *J. Mol. Liq.* **2019**, *279*, 224–231. [CrossRef]
4. Sekhon, B.S. Food nanotechnology-an overview. *Nanotechnol. Sci. Appl.* **2010**, *3*, 1–15. [PubMed]
5. Kordy, M.G.M.; Abdel-Gabbar, M.; Soliman, H.A.; Aljohani, G.; BinSabt, M.; Ahmed, I.A.; Shaban, M. Phyto-Capped Ag Nanoparticles: Green Synthesis, Characterization, and Catalytic and Antioxidant Activities. *Nanomaterials* **2022**, *12*, 373. [CrossRef]
6. Verma, V.; Al-Dossari, M.; Singh, J.; Rawat, M.; Kordy, M.G.M.; Shaban, M. A Review on Green Synthesis of TiO_2 NPs: Photocatalysis and Antimicrobial Applications. *Polymers* **2022**, *14*, 1444. [CrossRef]
7. Yuan, F.; Xia, Y.; Lu, Q.; Xu, Q.; Shu, Y.; Hu, X. Recent advances in inorganic functional nanomaterials based flexible electrochemical sensors. *Talanta* **2022**, *244*, 123419. [CrossRef]
8. González-González, R.B.; Rodríguez-Hernández, J.A.; Araújo, R.G.; Sharma, P.; Parra-Saldívar, R.; Ramirez-Mendoza, R.A.; Bilal, M.; Iqbal, H.M. Prospecting carbon-based nanomaterials for the treatment and degradation of endocrine-disrupting pollutants. *Chemosphere* **2022**, *297*, 134172. [CrossRef]
9. De Souza, F.M.; Gupta, R.K. Covalent Organic Frameworks-Based Nanomaterials for Hydrogen Evolution Reactions. In *Covalent Organic Frameworks*; CRC Press: Boca Raton, FA, USA, 2022; pp. 153–170. [CrossRef]
10. Alanazi, A.T.; Rice, J.H. Hybrid composite based on conducting polymers and plasmonic nanomaterials applied to catalysis and sensing. *Mater. Res. Express* **2022**, *9*, 075002. [CrossRef]
11. Alsamhary, K.I. Eco-friendly synthesis of silver nanoparticles by Bacillus subtilis and their antibacterial activity. *Saudi J. Biol. Sci.* **2020**, *27*, 2185–2191. [CrossRef]
12. Miranda, R.R.; Sampaio, I.; Zucolotto, V. Exploring silver nanoparticles for cancer therapy and diagnosis. *Colloids Surf. B Biointerfaces* **2021**, *210*, 112254. [CrossRef]
13. Algotiml, R.; Gab-Alla, A.; Seoudi, R.; Abulreesh, H.H.; El-Readi, M.Z.; Elbanna, K. Anticancer and antimicrobial activity of biosynthesized Red Sea marine algal silver nanoparticles. *Sci. Rep.* **2022**, *12*, 2421. [CrossRef]
14. Naganthran, A.; Verasoundarapandian, G.; Khalid, F.E.; Masarudin, M.J.; Zulkharnain, A.; Nawawi, N.M.; Karim, M.; Abdullah, C.A.C.; Ahmad, S.A. Synthesis, Characterization and Biomedical Application of Silver Nanoparticles. *Materials* **2022**, *15*, 427. [CrossRef]
15. Narayanan, K.B.; Sakthivel, N. Biological synthesis of metal nanoparticles by microbes. *Adv. Colloid Interface Sci.* **2010**, *156*, 1–13. [CrossRef]
16. Huang, J.; Zhan, G.; Zheng, B.; Sun, D.; Lu, F.; Lin, Y.; Chen, H.; Zheng, Z.; Zheng, Y.; Li, Q. Biogenic Silver Nanoparticles by Cacumen Platycladi Extract: Synthesis, Formation Mechanism, and Antibacterial Activity. *Ind. Eng. Chem. Res.* **2011**, *50*, 9095–9106. [CrossRef]
17. Role of Microbes in Waste Recycling. Available online: https://sciencing.com/role-microbes-waste-recycling-8091838.html (accessed on 9 September 2022).
18. Gupta, J.; Tyagi, B.; Rathour, R.; Thakur, I.S. Microbial Treatment of Waste by Culture-Dependent and Culture-Independent Approaches: Opportunities and Challenges. *Microb. Divers. Ecosyst. Sustain. Biotechnol. Appl.* **2019**, *1*, 415–446. [CrossRef]
19. Dejohn, P.B.; Hutchins, R.A. Treatment of dye wastes with granular activated carbon. *Text. Chem. Colorist* **1976**, *8*, 34–38.
20. Schneider, C.A.; Rasband, W.S.; Eliceiri, K.W. NIH Image to ImageJ: 25 Years of image analysis. *Nat. Methods* **2012**, *9*, 671–675. [CrossRef]
21. Inbakandan, D.; Venkatesan, R.; Khan, S.A. Biosynthesis of gold nanoparticles utilizing marine sponge Acanthella elongata (Dendy, 1905). *Colloids Surf. B Biointerfaces* **2010**, *81*, 634–639. [CrossRef]
22. Alfryyan, N.; Kordy, M.G.M.; Abdel-Gabbar, M.; Soliman, H.A.; Shaban, M. Characterization of the biosynthesized intracellular and extracellular plasmonic silver nanoparticles using *Bacillus cereus* and their catalytic reduction of methylene blue. *Sci. Rep.* **2022**, *12*, 12495. [CrossRef]
23. Taboada-López, M.V.; Bartczak, D.; Cuello-Núñez, S.; Goenaga-Infante, H.; Bermejo-Barrera, P.; Moreda-Piñeiro, A. AF4-UV-ICP-MS for detection and quantification of silver nanoparticles in seafood after enzymatic hydrolysis. *Talanta* **2021**, *232*, 122504. [CrossRef] [PubMed]

24. Picoli, S.U.; Durán, M.; Andrade, P.F.; Duran, N. Silver nanoparticles/silver chloride (Ag/AgCl) synthesized from Fusarium oxysporum acting against Klebsiella pneumouniae carbapenemase (KPC) and extended spectrum beta-lactamase (ESBL). *Front. Nanosci. Nanotechnol.* **2016**, *2*, 107–110. [CrossRef]
25. Paulkumar, K.; RajeshKumar, S.; Gnanajobitha, G.; Vanaja, M.; Malarkodi, C.; Annadurai, G. Biosynthesis of Silver Chloride Nanoparticles Using Bacillus subtilis MTCC 3053 and Assessment of Its Antifungal Activity. *ISRN Nanomater* **2013**, *2013*, 1–8. [CrossRef]
26. Wu, F.; Wang, W.; Xu, Z.; Li, F. Bromide (Br)-Based Synthesis of Ag Nanocubes with High-Yield. *Sci. Rep.* **2015**, *5*, 10772. [CrossRef] [PubMed]
27. Sharifi-Rad, M.; Pohl, P. Synthesis of Biogenic Silver Nanoparticles (AgCl-NPs) Using a Pulicaria vulgaris Gaertn. Aerial Part Extract and Their Application as Antibacterial, Antifungal and Antioxidant Agents. *Nanomaterials* **2020**, *10*, 638. [CrossRef]
28. Lou, Z.; Huang, B.; Wang, P.; Wang, Z.; Qin, X.; Zhang, X.; Cheng, H.; Zheng, Z.; Dai, Y. The synthesis of the near-spherical AgCl crystal for visible light photocatalytic applications. *Dalton Trans.* **2011**, *40*, 4104–4110. [CrossRef]
29. Altowyan, A.S.; Shaban, M.; Abdelkarem, K.; El Sayed, A.M. The Impact of Co Doping and Annealing Temperature on the Electrochemical Performance and Structural Characteristics of SnO_2 Nanoparticulate Photoanodes. *Materials* **2022**, *15*, 6534. [CrossRef]
30. Altowyan, A.S.; Shaban, M.; Abdelkarem, K.; El Sayed, A.M. The Influence of Electrode Thickness on the Structure and Water Splitting Performance of Iridium Oxide Nanostructured Films. *Nanomaterials* **2022**, *12*, 3272. [CrossRef]
31. Mohamed, H.S.; Rabia, M.; Zhou, X.-G.; Qin, X.-S.; Khabiri, G.; Shaban, M.; Younus, H.A.; Taha, S.; Hu, Z.-Y.; Liu, J.; et al. Phase-junction Ag/TiO2 nanocomposite as photocathode for H2 generation. *J. Mater. Sci. Technol.* **2021**, *83*, 179–187. [CrossRef]
32. Shaban, M.; El Sayed, A.M. Influence of the spin deposition parameters and La/Sn double doping on the structural, optical, and photoelectrocatalytic properties of CoCo2O4 photoelectrodes. *Sol. Energy Mater. Sol. Cells* **2020**, *217*, 110705. [CrossRef]
33. Chishti, A.N.; Ni, L.; Guo, F.; Lin, X.; Liu, Y.; Wu, H.; Chen, M.; Diao, G.W. Magnetite-Silica core-shell nanocomposites decorated with silver nanoparticles for enhanced catalytic reduction of 4-nitrophenol and degradation of methylene blue dye in the water. *J. Environ. Chem. Eng.* **2021**, *9*, 104948. [CrossRef]